Preprints of the 21st IFAC World Congress (Virtual)
Berlin, Germany, July 12-17, 2020

Multi-Modes Control for Semi-Active Suspension Systems

G. BEL HAJ FREJ [*,***] **X. MOREAU** [*,***]
E. HAMROUNI [*,**,***] **A. BENINE-NETO** [*,***]
V. HERNETTE [**,***]

[*] *IMS Lab, CNRS UMR 5218, Bordeaux INP, Univ. Bordeaux, France.*
[**] *Groupe PSA, 2 route de Gisy, 78943 Vlizy-Villacoublay*
[***] *OpenLab PSA-IMS 'Electronics and Systems for Automotive'*

(e-mails: ghazibelhajfrej@yahoo.fr ; xavier.moreau@u-bordeaux.fr ; emna.hamrouni@u-bordeaux.fr ; andre.benine-neto@u-bordeaux.fr ; vincent.hernette@mpsa.com)

Abstract: The aim of this work is to design and analyze multi-modes semi-active suspension using a Continuously Variable Damper (CVD). A modeling approach for the CVD is presented, and three suspension modes are developed. The studied damper can achieve different suspension modes by controlling the actuation force, which makes its damping adjustment more efficient. By applying an appropriate control strategy to the damper based on minimizing the quadratic gap between the control actuation force for each mode and a control target, satisfaction of both ride comfort and driving safety can be realized. The control target is synthesized using CRONE-SkyHook approach. Performances of the proposed method are validated through a speed bump profile and a real measured road profile.

Keywords: Vehicle Suspension, Semi-Active Suspension Control, Multi-mode, Control Strategy, CRONE, SkyHook.

1. INTRODUCTION

Vehicle suspension should be able to ensure different performances on the aspects of vibratory isolation, road handling and ride comfort (Hamrouni et al. (2019)). Based on the external power input, vehicle suspension can be classified on three categories: passive, semi-active and active. Semi-active suspensions have been extensively studied because of their high performances when compared to the passive ones, and the low energy consumption when compared to active ones (Jialing et al. (2006)).

Since 1980, several studies have been conducted to develop semi-active suspension using Continuously Variable Dampers (CVD) (Ivers and Miller (1989); Heo and Son (2003)). A CVD can yields variable damping force at a given damper velocity. Thus, it is possible to obtain a satisfaction of driving comfort and driving safety by adopting an appropriate implementable algorithm. Different types of CVD, such as electromagnetic actuators (Gysen et al. (2010)), pneumatic actuators (Bouvin et al. (2017)), and hydropneumatic actuators (Rizzo et al. (2009)), are often considered as the actuator of the damping adjustment. Many existent methods focused on developing a practical, implementable and lower cost control scheme (Liu et al. (2019)). These methods include SkyHook control, Groundhook control, Hybrid control, PID control, Fuzzy logic control... The most implemented controller from a commercial point of view is the SkyHook damping concept.

Although CVD can realize greatly adjustable characteristics, a small damping variation doesn't significantly influence the control performances of a suspension system (Chen et al. (2013); Sun et al. (2017)). Therefore, a CVD with multiple damping modes achieved by a simple control strategy and a reliable regulation mechanism may be more reliable and efficient (Wei and Zhiqiang (2019)).

Compared with the conventional semi-active suspension using CVD, the aim of this study is to design a new semi-active suspension with different damping modes. Each suspension mode ensure either vibratory isolation or chassis holding. By just comparing the damper efforts of each mode with a target one, multi-mode switching damping characteristics are achieved. A Robust Control Frequency Synthesis (CRONE) technique (Moreau et al. (1999)), combined with the SkyHook one, are used to synthesize the target mode that satisfy both vibratory isolation and chassis holding.

The remainder of this paper is organized as follows. Section 2 details the analysis and design scheme for a quarter-car vehicle suspension model. Section 3 presents the design methodology of the three suspension modes. The CRONE-SkyHook approach used to design the target effort for the semi-active damper, and the switching control strategy, are described in section 4. In section 5, simulation results are presented to show the performance of the proposed

[1] *This work took place in the framework of the OpenLab 'Electronics and Systems for Automotive' combining IMS laboratory and PSA Groupe company.

switching strategy. Finally, conclusions are given in section 6.

2. VEHICLE SUSPENSION MODELING

2.1 Analysis and design method

Results presented in this paper are part of the hierarchical chassis control of an autonomous vehicle for which the operating domain is divided into three sub-domains: low-frequency comfort, road behavior and active safety in emergency situations (Bouvin et al. (2018)). This study concerns the low-frequency comfort domain which corresponds to the range $[0.5, 5.5]$ Hz for vertical dynamics, and for horizontal dynamics to longitudinal and transverse accelerations lower than $|0.4|$ g. The vertical dynamics has no significant influence on the horizontal dynamics in this field. A two degrees of freedom (2-DOF) quarter vehicle model instead of the 14-DOF can then be used in the exploratory phase. Note that we dispose of a 14-DOF vehicle model operating in MATLAB/Amesim co-simulation and used for validation before implantation and vehicle test.

A full car model can be simplified to the well known quarter vehicle model. Fig. 1 shows the quarter-car model with 2-DOF, reflecting the Chassis/Road transfer in the range of $[0.5, 5.5]Hz$, where m_1 is the unsprung mass, $z_1(t)$ is its displacement and $v_1(t)$ its velocity, m_2 is the sprung mass, $z_2(t)$ is its displacement and $v_2(t)$ its velocity, k_1 is the vertical stiffness of the tire, k_2 is the stiffness coefficient of the suspension, b_1 is the damping coefficient of the tire, b_2 is the damping coefficient of the suspension. $f_0(t)$ and $v_0(t)$ are respectively the load transfer and the road vertical excitation applied to the quarter-vehicle.

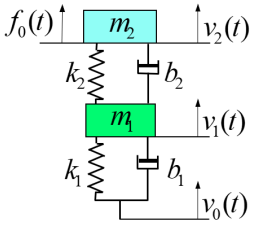

Fig. 1. Quarter-car vehicle suspension model.

The block-diagram shown in Fig. 2 issued from the quart vehicle model highlights the preponderant role of suspension, modeled by the impedance $I_s(s)$ and the admittance $A_2(s)$ (Rizzo et al. (2009)). The suspension impedance I_s,

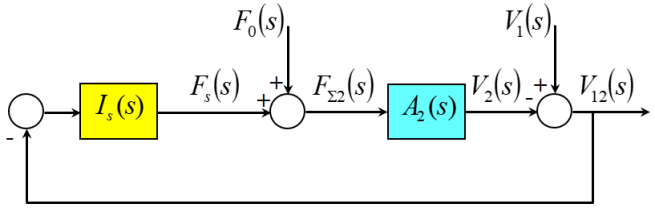

Fig. 2. Block-diagram of the loop.

between the suspension force $F_s(s)\,[N]$ and the deflection velocity $V_{12}(s)\,[m/s]$, is given by

$$I_s(s) = \frac{F_s(s)}{V_{12}(s)} = \frac{k_2}{s} + b_2, \tag{1}$$

where

$$V_{12}(s) = V_1(s) - V_2(s). \tag{2}$$

The admittance $A_2(s)$ between $F_{\Sigma 2}(s)\,[N]$, the algebraic sum of the forces applied to m_2, and the velocity $V_2\,[m/s]$, is expressed by

$$A_2(s) = \frac{V_2(s)}{F_{\Sigma 2}(s)} = \frac{1}{m_2 s}. \tag{3}$$

The open loop transfer function $\beta(s)$, expressed by the product of the impedance of the suspension and the admittance of the sprung mass $A_2(s)$ is

$$\beta(s) = I_s(s)A_2(s) = \frac{V_2(s)}{V_1(s) - V_2(s)}|_{F_0=0}. \tag{4}$$

After development, the transfer function $\beta(s)$ can be written in the following form:

$$\beta(s) = \left(1 + \frac{s}{w_2}\right)\left(\frac{w_{n2}}{s}\right)^2, \tag{5}$$

where

$$w_2 = \frac{k_2}{b_2}\ ;\quad w_{n2} = \sqrt{\frac{k_2}{m_2}} \tag{6}$$

The transfer function between the suspension effort $F_s(s)$ and the sprung force $F_k(s)$ is

$$\frac{F_s(s)}{F_k(s)} = D_s(s) = \left(1 + \frac{s}{w_2}\right). \tag{7}$$

Using the Laplace variable s equals $j\omega$, the gain and the phase of $D_s(j\omega)$ in the frequency domain are expressed respectively by

$$\rho\,(\omega) = |D_s\,(j\omega)\,| = 1 + j\frac{\omega}{\omega_2} = \sqrt{1 + \left(\frac{\omega}{\omega_2}\right)^2} \tag{8a}$$

$$\phi\,(\omega) = arg\,[D_s\,(j\omega)] = arg|1 + j\frac{\omega}{\omega_2}| = arctg\left(\frac{\omega}{\omega_2}\right). \tag{8b}$$

Add to that, the transfer in absolute transmission $T_{21}(s)$

$$T_{21}(s) = \frac{Z_2(s)}{Z_1(s)} = \frac{V_2(s)}{V_1(s)} = \frac{\beta(s)}{1 + \beta(s)}. \tag{9}$$

Then, to specify the resonance peak Q_2 of the frequency response of $T_{21}(j\omega)$, a phase margin should be imposed to the transfer $\beta(j\omega)$.

The phase margin M_ϕ calculated at the proper angular frequency w_{n2} of the sprung mass m_2 is defined as follows:

$$\begin{aligned} M_\phi &= \pi + arg\,(\beta(j\omega_{n2})) \\ &= \pi + arg\left(1 + \frac{j\omega_{n2}}{w_2}\right) + arg\left(\frac{\omega_{n2}}{j\omega_{n2}}\right)^2. \end{aligned} \tag{10}$$

Let the phase

$$\phi = arg\left(1 + \frac{j\omega_{n2}}{\omega_2}\right) \geq 0, \tag{11}$$

and knowing that

$$arg\left(\frac{w_{n2}}{j\omega_{n2}}\right)^2 = -\pi, \tag{12}$$

it results

$$M_\phi = \pi + \phi - \pi \Rightarrow \phi \approx M_\phi. \tag{13}$$

If the requirement resonant peak is chosen to be $Q_2 \leq 2$, the phase margin M_ϕ should be

$$M_\phi > 40°. \tag{14}$$

So, the vehicle holding is directly linked to the phase lead provided by the $D_s(j\omega)$ in the vicinity of ω_{n2}.

2.2 Metallic suspension

The metallic suspension is taken as a benchmarking system in this study. So, relations between different variable parameters should be defined in term of transfer functions.

The transfer function between $Z_2(s)$ and $Z_0(s)$ is

$$\frac{Z_2(s)}{Z_0(s)} = \frac{(b_1 s + k_1)(b_2 s + k_2)}{den(s)}, \tag{15}$$

where

$$\begin{aligned} den(s) = {} & m_1 m_2 s^4 + (m_2(b_1 + b_2) + m_1 b_2) s^3 \\ & + (m_2(k_1 + k_2) + m_1 k_2 + b_1 b_2) s^2 \\ & + (k_1 b_2 + b_1 k_2) s + k_1 k_2 \end{aligned} . \tag{16}$$

The transfer function Z_1/Z_0 is defined by

$$\frac{Z_1(s)}{Z_0(s)} = \frac{(b_1 s + k_1)(m_2 s^2 + b_2 s + k_2)}{den(s)}. \tag{17}$$

The transfer function Z_2/F_0 is equal to

$$\frac{Z_2(s)}{F_0(s)} = \frac{(m_1 s^2 + (b_1 + b_2) s + (k_1 + k_2))}{den(s)}. \tag{18}$$

Parametric variables of the metallic suspension are chosen to be those of *Citroën C4 Picasso* (Table 1). The viscous damping coefficient b_2 is fixed to obtain a resonance factor $Q_2 = 2$.

Table 1: *Citroën C4 Picasso* parameters

Setting	Values	Units
m_1	41.3	kg
m_2	271	kg
k_2	26043	N/m
k_1	300000	N/m
b_2	1875	Ns/m
b_1	50	Ns/m
ω_{n1}	88.85	rad/s
ω_{n2}	9.81	rad/s
ξ_2,	0.353	
ξ_1	0.262	

Note that the damping of the wheel dynamic is defined by

$$\xi_1 = \frac{b_1 + b_2}{2\sqrt{(k_1 + k_2) m_1}}, \tag{19}$$

and the damping of the chassis dynamic is

$$\xi_2 = \frac{b_2}{2\sqrt{k_2 m_2}}. \tag{20}$$

3. CONTROL OF MULTI-MODES SEMI-ACTIVE SUSPENSION

The studied suspension system is composed of passive metallic spring damper units associated to actuators enabling the vehicle high regulation. b_{20} is the damping coefficient of the passive damper and F_a is the controlled actuation force (Fig. 3-Functional Level).

The suspension force is then described by the following equation

$$F_s(s) = \left(\frac{k_2}{s} + b_{20}\right) V_{12}(s) + F_a(s). \tag{21}$$

3.1 Degraded mode suspension

For passive suspension, the actuation F_a equals zero and hence the force suspension (21) is equal to

$$F_s(s) = \left(\frac{k_2}{s} + b_{20}\right) V_{12}(s). \tag{22}$$

This mode is dimensioned to ensure a minimal wheel holding. For that, b_{20} should be computed to guarantee a maximal resonance factor $Q_1 = 3$ of the frequency response Z_1/Z_0 of the tyre, and therefore a minimum damping factor $\xi_1 = 0.15$.

For the passive suspension design, a high damping coefficient b_{20} is required to attenuate the peak of the sprung mass resonance. However, high frequency attenuation is degraded in this case.

3.2 Multi-modes semi-active suspension

For a component point of view, the quarter-car semi-active suspension system can be modeled as described in Fig. 3,

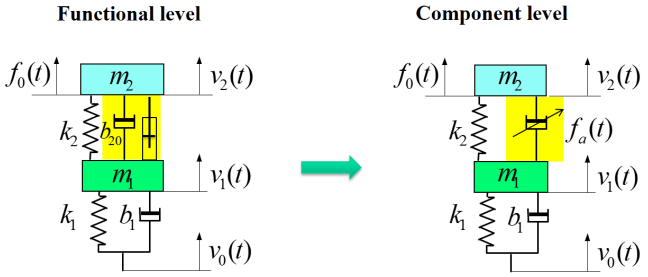

Fig. 3. From Functional level to Component level.

where

$$f_a(t) = b(t) v_{12}(t). \tag{23}$$

According to the concrete structure of damper, three modes of the damper based on the control actuation force can be summarized:

- 'Mode 1' is designed to ensure vibration isolation performances;
- 'Mode 2' is equivalent to the metallic suspension;
- 'Mode 3' is modeled to ensure chassis holding.

The equivalent expressions of the control actuation force f_a for each mode are as follows

$$\begin{cases} f_{a_1}(t) = b_{20} v_{12}(t) \\ f_{a_2}(t) = b_2 v_{12}(t) \\ f_{a_3}(t) = b_3 v_{12}(t) \end{cases} . \tag{24}$$

The domain of definition of each mode is detailed in Fig. 4.

where

$$f_{a_{max}}(t) = \begin{cases} a_0 v_{12}(t) & , \forall \|v_{12}(t)\| < v_{lim} \\ sign(v_{12}(t)) f_{a_0} + a_1 (v_{12}(t) - v_{lim}) & , \forall \|v_{12}(t)\| \geq v_{lim} \end{cases} \tag{25a}$$

$$f_{a_{min}}(t) = b_{20} v_{12}(t), \tag{25b}$$

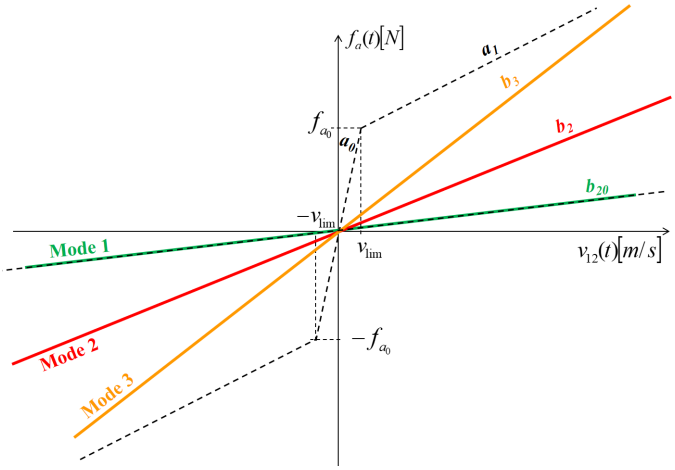

Fig. 4. The variation ranges of the suspension efforts for the three suspension modes.

are the upper and the lower bound of the suspension effort, respectively. Note that $f_{a_{max}}$ and $f_{a_{min}}$ are issued from the technical documentation of the CVD, implemented in PSA commercialized vehicles. This CVD is electrically piloted in order to obtain 'Mode 1' and 'Mode 2'.

Fig. 5 presents a comparison between frequency responses $Z_2(j\omega)/Z_0(j\omega)$ of the three suspension modes in the range $[0.5, 5.5]Hz$.

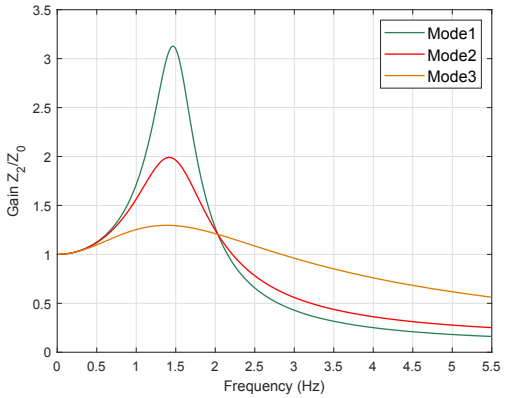

Fig. 5. Comparisons between frequency responses Z_2/Z_0 of three suspension modes.

As expected, none of the architectures can ensure the best chassis holding and the best vibratory isolation at the same time. However, each mode (from 1 to 3) has a frequency range where it provides better performances as shown in Fig. 5.

4. AUTOMATIC CONTROL STRATEGY

4.1 CRONE-SkyHook based target effort

In this section, the aim is to synthesize a target mode which can improve both chassis holding and vibratory isolation in a very significant way. For that, a CRONE-SkyHook strategy is used. An additional controller $C_{csh}(s)$ is added to the quarter-car model (Fig. 6).

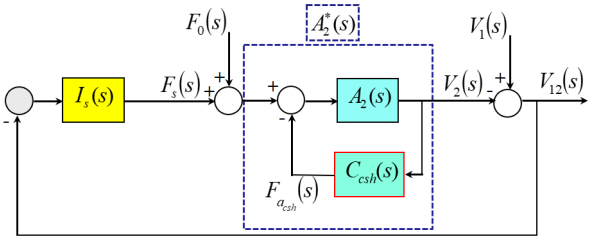

Fig. 6. Generalized schema of the loop.

The impedance of the additional system is

$$C_{csh}(s) = \frac{F_{a_{csh}}(s)}{V_2(s)} = \frac{b_{csh}}{\left(1 + \frac{s}{\omega_n}\right)^n}, \tag{26}$$

where $n \in \mathbb{R}^+$ and b_{csh} is the control parameter to be synthesized. In order to facilitate comparison with the traditional SkyHook method, the order n is set to zero. $C_{csh}(s)$ is chosen to be a low pass filter in order to act for chassis holding and limit the action of b_{csh} in low frequency.

Then, the modified impedance of the sprung mass becomes

$$A_2^\star(s) = \frac{1}{m_2 s + C_{csh}(s)}. \tag{27}$$

By supposing $n = 0$, the open-loop transfer $\beta^\star(s)$ is expressed by

$$\begin{aligned} \beta^\star(s) &= \left(\frac{k_2}{s} + b_{20}\right)\left(\frac{1}{m_2 s + C_{csh}(s)}\right) \\ &= \frac{\omega_1}{s}\left(\frac{1 + \frac{s}{\omega_{2_0}}}{1 + \frac{s}{\omega_3}}\right) \end{aligned}, \tag{28}$$

where

$$\omega_1 = \frac{k_2}{b_{csh}} \;;\; \omega_{2_0} = \frac{k_2}{b_{2_0}} \;;\; \omega_3 = \frac{b_{csh}}{m_2} \tag{29}$$

Supposing that

$$\omega_{2_0} = \omega_3, \tag{30}$$

then $\beta^\star(s)$ becomes

$$\beta^\star(s) = \frac{\omega_1}{s}, \tag{31}$$

and the new transfer in absolute transmission $T_{21}^\star(s)$ becomes

$$T_{21}^\star(s) = \frac{1}{1 + \frac{s}{\omega_1}}. \tag{32}$$

From (28),(30) and (31), it results

$$b_{csh} = \frac{k_2 m_2}{b_{2_0}}. \tag{33}$$

Finally, the target effort designed by the CRONE-SkyHook strategy is

$$f_{a_{csh}}(t) = b_{csh} v_{12}(t). \tag{34}$$

Remark 1: Note that this result can only be achieved with an active device (which is not the case here). The interest therefore lies in the simplicity of the calculation of the target effort $f_{a_{csh}}(t)$ which leads to a Chassis/Road frequency response which is sufficiently discriminating compared to the frequency responses of each of the three modes (Fig. 7).

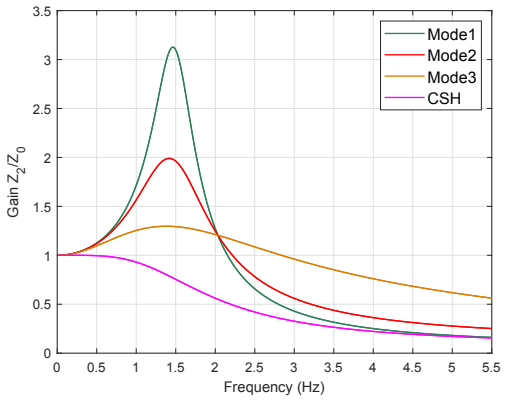

Fig. 7. Comparison between control effort for the three suspension modes and CRONE-SkyHook target effort.

4.2 Decision criterion

The choice of the specified mode, and hence of the control, can be done by minimizing the quadratic difference between a target effort and the predicted effort for each suspension modes. It is therefore sufficient to switch at each step time to the mode which has the smallest gap with the target effort. Thus, the gap $\mathcal{G}$ between the target effort and the efforts is defined a following:

$$\mathcal{G} = \begin{bmatrix} \left(f_{a_{target}}(t) - f_{a_1}(t)\right)^2 \\ \left(f_{a_{target}}(t) - f_{a_2}(t)\right)^2 \\ \left(f_{a_{target}}(t) - f_{a_3}(t)\right)^2 \end{bmatrix}. \tag{35}$$

where $f_{a_{target}} = f_{a_{csh}}$ is synthesized with the CRONE-SkyHook strategy.

Remark 2: The dynamics of the actuator is an important factor that affects the operation performance of the multi-modes semi-active suspension system. To improve the control performance of the proposed control scheme, the dynamic of the actuator is modeled as a second order filter with $60ms$ of response time.

5. PERFORMANCE COMPARISON

5.1 Isolated Obstacle

Simulation in time domain were carried out for a vehicle driving over a speed bump at $V_x = 15km/h$. The geometric profile of the obstacle is defined as follows

$$\begin{cases} z_0(x) &= \dfrac{h}{2}(tanh(a(x - x_0)) - tanh(a(x - (x_0 + L))) \\ x(t) &= V_x t \\ a &= \dfrac{2}{h} tan\alpha \end{cases}, \tag{36}$$

where $x_0 = 5m$ is the position of the first inflection point, $L = 30m$ is length between the two inflection points, $h = 0.01m$ is the height of the obstacle and $\alpha = 10°$ is the approach angle at the inflection point.

The isolated obstacle is used to check the coherence of the temporal results with the frequency results. Thus, the length of the obstacle is defined in such a way that the transitional regime of the climb phase is completed before going on to the transitional regime of the descent phase. Thus, the duality between time and frequency domain can be checked.

Fig. 8 shows the dynamic of the chassis displacement for the whole length of the obstacle, where z_0 is the speed bump profile, z_{2_i}, $i = 1, 2, 3$ are the body displacement related to the three suspension modes, $z_{2_{csh}}$ is the body displacement issued from the use of the CRONE-SkyHook controller, and z_2 is the resulted body displacement using the switched control scheme.

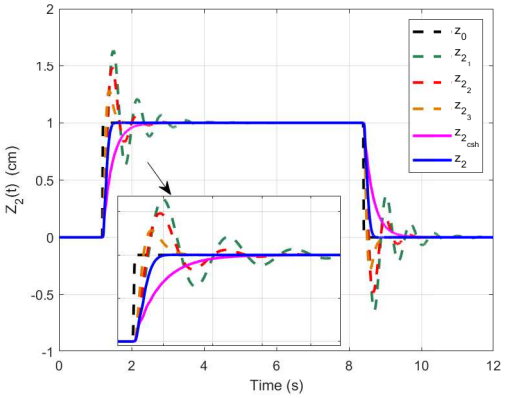

Fig. 8. Time responses of the body displacement $z_2(t)$.

The zoom in the transitional regime of the climb phase shows that, in the first steps, the vibratory isolation is improved. Then, a reduction of the first overshoot and a decrease of the oscillatory nature of the response $z_2(t)$ are obtained with the piloted suspension, an thus chassis holding is improved. Note that the piloted suspension is chosen to be initialized with the 'mode 2'.

Fig. 9 presents the target effort $f_{a_{csh}}$, the resulted effort f_a, as well as efforts of the three suspension modes which are predicted at each instant and then used for the decision test. It can be seen from Fig. 9 that the resulted f_a is acceptable compared to the predicted ones.

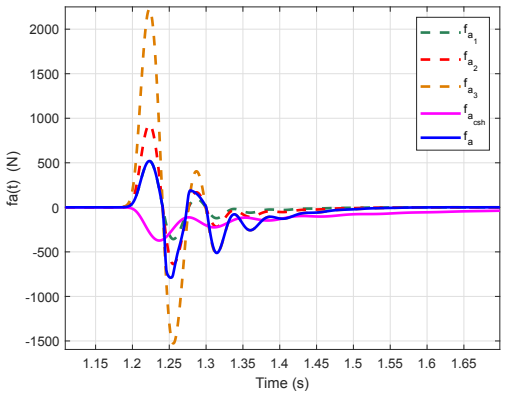

Fig. 9. Suspension forces at the transitional regime of the climb phase.

The analysis of the cumulative time per mode shows that that the third mode of suspension ensuring chassis holding, is predominant for such type of obstacle.

5.2 Road profile

A stochastic road excitation is used to validate performances of the proposed multi-modes semi-active suspension using a CVD. The used road profile is measured with a constant vehicle speed of $60km/h$.

Fig. 10 describes the controlled vertical displacement $z_2(t)$ and compared to the measured road $z_0(t)$. A performance indicator based on the Root Mean Square (RMS) can be calculated for the entire duration of the profile:

$$J = \frac{RMS\left[z_2(t)\right]}{RMS\left[z_0(t)\right]}, \tag{37}$$

where $RMS\left[z_2(t)\right]$ is the root mean square of the vertical displacement $z_2(t)$, calculated for the benchmarking metal suspension and for the controlled suspension, and then normalized by $RMS\left[z_0(t)\right]$ (the root mean square of the measured road $z_0(t)$).

A such criterion can be interpreted as following

- $J > 1 \rightarrow$ an amplified transmission;
- $J = 1 \rightarrow$ a neutral transmission;
- $J < 1 \rightarrow$ an attenuated transmission.

The value of the performance indicator for this road profile is $J = 0.9652$. Thus, the piloted suspension has improved the vibratory isolation.

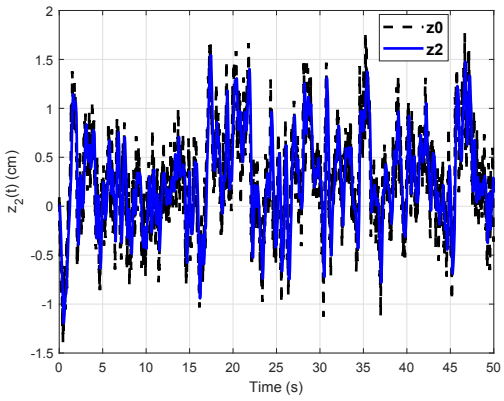

Fig. 10. Comparison between time responses of the vertical displacement $z_2(t)$ and the measured road $z_0(t)$.

The analysis of the histogram of commutations for the measured road profile shows that 'mode 1' is dominant. Thus, the vibratory isolation is predominant during this road profile.

6. CONCLUSION

In this study, a continuously variable damper with three suspension modes has been proposed for semi-active vehicle suspension. By simply controlling the actuating force, the damper can achieve effectively adjustable damping and meet the set requirements as ride comfort and driving safety. The control strategy is based on the minimization of the quadratic difference between the control actuation force for the three suspension modes, and a target developed by a new CRONE-SkyHook technique. Numerical simulations are used to validate the performance of the proposed semi-active suspension. Results show that the control strategy can effectively improve vehicle ride comfort and safety performances. Future works will focus on road behavior and active safety in emergency situations of autonomous vehicle.

REFERENCES

Bouvin, J., Hamrouni, E., Moreau, X., Benine-Neto, A., Hernette, V., Serrier, P., and Oustaloup, A. (2018). Hierarchical approach for global chassis control. In *2018 European Control Conference (ECC)*, 2555–2560.

Bouvin, J.L., Moreau, X., Benine-Neto, A., Oustaloup, A., Serrier, P., and Hernette, V. (2017). CRONE control of a pneumatic self-leveling suspension system. *IFAC-PapersOnLine*, 50(1), 13816 – 13821. 20th IFAC World Congress.

Chen, L., Yu, L., and Cui, X. (2013). Performance simulation and testing of multi-levels-damping adjustable hydraulic shock absorber. *Journal of Jiangsu University (Natural Science Edition)*, 34, 249–253.

Gysen, B.L.J., Paulides, J.J.H., Janssen, J.L.G., and Lomonova, E.A. (2010). Active electromagnetic suspension system for improved vehicle dynamics. *IEEE Transactions on Vehicular Technology*, 59(3), 1156–1163.

Hamrouni, E., Moreau, X., Benine-Neto, A., and Hernette, V. (2019). Skyhook and CRONE active suspensions: A comparative study. *9th IFAC Symposium on Advances in Automotive Control AAC 2019*, 52(5), 243 – 248.

Heo, S.J. and Son, S.H. (2003). Modelling of continuously variable damper for design of semi-active suspension systems. *International Journal of Vehicle Design - INT J VEH DES*, 31.

Ivers, D.E. and Miller, L.R. (1989). Experimental comparison of passive, semi-active on/off, and semi-active continuous suspensions. In *SAE Technical Paper*. SAE International.

Jialing, Y., Weiyi, C., and Ning, C. (2006). A review on the development status of automotive semi-active suspension systems. *Automotive Engineering*, 28(3), 276–280.

Liu, C., Chen, L., Yang, X., Zhang, X., and Yang, Y. (2019). General theory of skyhook control and its application to semi-active suspension control strategy design. *IEEE Access*, 7, 101552–101560.

Moreau, X., Oustaloup, A., and Nouillant, M. (1999). From analysis to synthesis of vehicle suspensions: The CRONE approach. In *1999 European Control Conference (ECC)*, 4094–4099.

Rizzo, A., Moreau, X., Oustaloup, A., and Hernette, V. (2009). A New CRONE Suspension: More Compact and More Efficient: Part 1Problematics and Specifications. volume 4, 1095–1102.

Sun, X., Yuan, C., Cai, Y., Wang, S., and Chen, L. (2017). Model predictive control of an air suspension system with damping multi-mode switching damper based on hybrid model. *Mechanical Systems and Signal Processing*, 94, 94 – 110.

Wei, T. and Zhiqiang, L. (2019). Damping multimode switching control of semiactive suspension for vibration reduction in a wheel loader. *Shock and Vibration*, 2019.